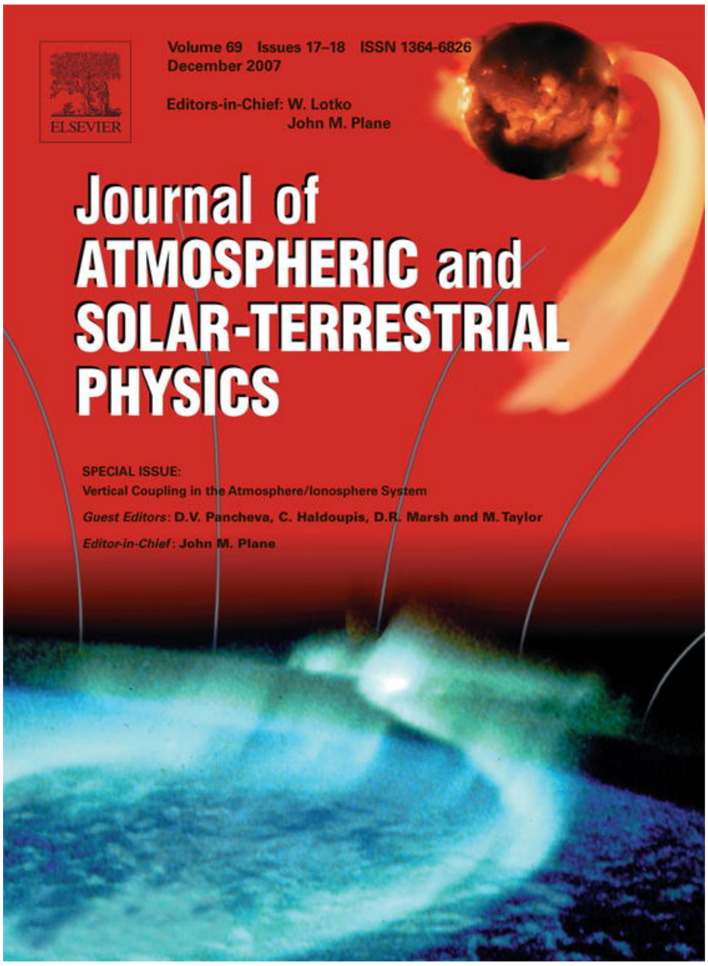
Volume 69 Issues 17–18 ISSN 1364-6826
December 2007
Editors-in-Chief: W. Lotko
John M. Plane
ELSEVIER
Journal of ATMOSPHERIC and SOLAR-TERRESTRIAL PHYSICS
SPECIAL ISSUE:
Vertical Coupling in the Atmosphere/Ionosphere System
Guest Editors: D.V. Pancheva, C. Haldoupis, D.R. Marsh and M. Taylor
Editor-in-Chief: John M. Plane

ELSEVIER

Journal of Atmospheric and Solar-Terrestrial Physics 69 (2007) 2203–2218

Journal of ATMOSPHERIC AND SOLAR-TERRESTRIAL PHYSICS

www.elsevier.com/locate/jastp

A climatology of nonmigrating semidiurnal tides from TIMED Doppler Interferometer (TIDI) wind data

J. Oberheide[a,*], Q. Wu[b], T.L. Killeen[b], M.E. Hagan[b], R.G. Roble[b]

[a]*Physics Department, University of Wuppertal, 42097 Wuppertal, Germany*
[b]*High Altitude Observatory, National Center for Atmospheric Research, Boulder, CO, USA*

Received 30 January 2007; received in revised form 25 April 2007; accepted 21 May 2007
Available online 2 June 2007

Abstract

With the launch of the TIMED satellite in December 2001, continuous temperature and wind data sets amenable to MLT tidal analyses became available. The wind measuring instrument, the TIMED Doppler Interferometer (TIDI), is operating since early 2002. Its day- and nighttime capability allows to derive tidal winds over a range of MLT altitudes. This paper presents climatologies (June 2002–June 2005) of monthly mean amplitudes and phases for six nonmigrating semidiurnal tidal components between 85 and 105 km altitude and between 45°S and 45°N latitude (westward propagating wave numbers 4, 3, 1; the standing oscillation s0; and eastward propagating wave numbers 1, 2) in the zonal and meridional wind directions.

Amplitude errors are 15–20% (accuracy) and 0.8 m/s (precision). The phase error is 2 h. The TIDI analysis agrees well with 1991–1994 UARS results at 95 km. During boreal winter, amplitudes of a single component can reach 10 m/s at latitudes equatorward of 45°. Aggregate effects of nonmigrating tides can easily reach or exceed the amplitude of the migrating tide. Comparisons with the global scale wave model (GSWM) and the thermosphere–ionosphere–mesosphere–electrodynamics general circulation model (TIME-GCM) are partly inconclusive but they suggest that wave–wave interaction and latent heat release in the tropical troposphere both play an important role in forcing the semidiurnal westward 1, westward 3, and standing components. Latent heat release is the leading source of the eastward propagating components.

Keywords: MLT winds; Nonmigrating semidiurnal tides; TIDI; TIMED; GSWM; TIME-GCM

1. Introduction

Atmospheric tides are global waves in temperature, winds, and density with periods that are harmonics of a solar day. They propagate up and away from their mostly tropospheric and stratospheric sources and transport energy and momentum from the lower into the middle and upper atmosphere. Hence, they are essential for understanding vertical coupling processes and for the dynamics, chemistry, and energetics of Earth's atmosphere. Tidal wind oscillations in the mesosphere and lower thermosphere (MLT) region dominate the meridional wind field and are on the order of the time-averaged zonal wind. Air parcels

*Corresponding author. Tel.: +49 202 439 2750.
E-mail address: joberh@uni-wuppertal.de (J. Oberheide).
URL: http://www.atmos.physik.uni-wuppertal.de (J. Oberheide).

1364-6826/$ - see front matter
doi:10.1016/j.jastp.2007.05.010

may be transported some 1000 km in the horizontal and some kilometers in the vertical direction with simultaneous changes in the reaction rates of chemically active species associated with the temperature tides (Ward, 1999).

Tidal waves are grouped into two classes: (i) the Sun-synchronous (migrating) tides and (ii) the non-Sun-synchronous (nonmigrating) tides. Migrating tides propagate westward with the apparent motion of the Sun with a zonal wave number that equals their frequency in cycles per day. They are primarily driven by the absorption of solar infrared and ultraviolet radiation in tropospheric water and water vapor, and stratospheric ozone. Non-Sun-synchronous (nonmigrating) tides are the tidal components that do not follow the apparent westward propagation of the Sun, that is, they may propagate westward, eastward, or remain standing with zonal wave numbers that do not equal their frequencies (in cycles per day). Their leading sources are latent heat release in the tropical troposphere (Hagan and Forbes, 2002, 2003) and the nonlinear interaction between planetary waves and the migrating tide (Lieberman et al., 2004; Forbes et al., 2003; Oberheide et al., 2002; Hagan and Roble, 2001). Hence, nonmigrating tides manifest the influence of large-scale weather systems that cannot propagate through the tropopause into the middle and upper atmosphere. Recent ionospheric ultraviolet emission measurements by FUV-IMAGE and GUVI/TIMED indicate that the effects of nonmigrating tides extend well into the F-layer via a longitude modulation of the E-layer dynamo electric fields (Immel et al., 2006).

Triggered by the growing appreciation of their importance, nonmigrating tides have been the target of increasing research activities by both experimenters and modelers during the past few years. In this work, only nonmigrating tides of semidiurnal period are considered. For an overview of recent diurnal analyses, see Oberheide et al. (2006) and references therein.

Tidal and general circulation models have been used to study semidiurnal nonmigrating tidal sources and morphology (Ward et al., 2005; Mayr et al., 2005; Hagan and Forbes, 2003; Grieger et al., 2002; Yamashita et al., 2002). These simulations gave an idea of the latent heat and planetary wave–tidal interaction forcing mechanisms and the spatio-temporal amplitude and phase distributions. A quantitative assessment of the model predictions and the underlying parameterizations, however, is an open issue which is primarily due to the lack of observation-based tidal definitions. The few observational results indicate that the present model understanding is in fact more qualitative with frequent discrepancies in both tidal magnitudes and spatio-temporal distributions.

Nonmigrating semidiurnal tides have been analyzed from ground-based measurements in Antarctica (Baumgaertner et al., 2006; Lau et al., 2006; Hibbins et al., 2006; Murphy et al., 2003) thereby extending the earlier results of Forbes et al. (1999), at northern high latitudes (Wu et al., 2003) and at northern mid-latitudes (Pancheva et al., 2002). Climatological information about the global structure comes predominantly from satellite analyses. Amplitudes and phases have been recently derived from SABER and MLS temperature measurements (Forbes and Wu, 2006; Forbes et al., 2006; Zhang et al., 2006). Unfortunately, the analysis of nonmigrating semidiurnal tides in MLT winds has so far been limited to 95 km altitude based upon measurements from HRDI and WINDII onboard UARS (Huang and Reber, 2004; Manson et al., 2004; Cierpik et al., 2003; Angelats i Coll and Forbes, 2002).

With the launch of the TIMED satellite in December 2001, continuous wind data from the TIMED Doppler Interferometer (TIDI) instrument (Killeen et al., 2006) became available. TIDI winds are highly amenable to nonmigrating tidal analyses over a range of MLT altitudes. They have already been analyzed for nonmigrating diurnal tides in an earlier paper (Oberheide et al., 2006). The present work extends this analysis to the semidiurnal tides. Climatologies (June 2002–June 2005) of monthly mean amplitudes and phases are derived for six semidiurnal tidal components between 85 and 105 km altitude and between 45°S and 45°N latitude (westward propagating wave numbers 4, 3, 1; the standing oscillation s0; and eastward propagating wave numbers 1, 2) in the zonal and meridional wind directions. The TIDI climatologies are compared to HRDI and WINDII analyses from Angelats i Coll and Forbes (2002) at 95 km and to model simulations of the global scale wave model (GSWM, Hagan and Forbes, 2003) and the thermosphere–ionosphere–mesosphere–electrodynamics general circulation model (TIME-GCM, Roble and Ridley, 1994). This allows us to assess the model prediction capabilities and to study the tidal forcing mechanisms.

The paper is organized as follows. The TIDI data and the tidal analysis method are described in Section 2, including error estimates. Tidal climatologies are presented in Section 3 and compared to HRDI and WINDII analysis in Section 4. Model comparisons and tidal forcing mechanisms are discussed in Section 5. Concluding remarks are given in Section 6.

2. Data and analysis

2.1. TIDI measurements

The instrument onboard the TIMED satellite with the primary objective to measure winds in the MLT region is TIDI. It was developed and built by the University of Michigan. See Killeen et al. (2006) for an overview and recent results. The present nonmigrating tidal analysis covers the time period from June 2002 to June 2005. TIDI is a limb scanner that measures the daytime and nighttime neutral winds by monitoring the Doppler shift of the various upper atmosphere airglow layers. The four TIDI telescopes are orthogonally orientated (45° with respect to the orbit) such that wind vectors on both sides of the satellite track are measured (i.e., cold and warm sides). Because the viewing directions of the two telescopes on the same side of the spacecraft are perpendicular to one another, the same locations are observed with a time delay of a few minutes when the satellite moves forward. Data are taken from pole-to-pole with a vertical resolution of 2.5 km and an along track resolution of about 800 km.

Warm and cold side neutral wind vectors, that is, the zonal (eastward) and meridional (northward) wind components are calculated from the line-of-sight (LOS) winds measured in the two directions on the same side of the spacecraft. Two different schemes are employed by the University of Michigan and the National Center for Atmospheric Research (NCAR). See Killeen et al. (2006) for details. Briefly, the University of Michigan scheme linearly interpolates the samplings of each telescopes to an evenly spaced track angle grid and calculates the wind vectors at these grid points. The NCAR scheme simply pairs sampling locations from one telescope with the nearest neighbors from the other. Pairs must be less than 500 km apart to calculate wind vectors. The results of both schemes do not differ much. TIDI data used here are O_2 (0–0) band P9 wind vectors (level3, data versions 00_01 (2002), 01_01 to 01_03 (2003), 03_03 (2004), 03_04 (2005)) between 85 and 105 km altitude that were produced by NCAR. They may be downloaded from http://timed.hao.ucar.edu/tidi/.

TIDI has continuously taken data with one larger data gap in early 2003. The instrument operational performance has been nominal except for two anomalies that are now well understood: (1) higher than expected background white light and (2) ice deposition on cold surfaces. Instrumental modes and data analysis techniques have been adjusted to mitigate their effects on data quality (Killeen et al., 2006). These efforts reduced the noise level of individual wind profiles by 30%. They were previously assumed to be 30 m/s during the day and double that during the night (Oberheide et al., 2006).

For a given day and latitude, TIDI measures at four different local solar times (LSTs) equatorward of ±60° and at two different LSTs poleward of ±60°. The TIMED orbit geometry results in a daily LST variation of 12 min toward earlier LST as time progresses. Hence, LSTs of measurements taken on the ascending (asc) and descending (dsc) parts of the orbit can be considered to be longitude independent for warm and cold side data, respectively. Complete (24 h) LST coverage is obtained every 60 days which corresponds to one satellite yaw cycle. The specifics of TIDI, particularly its day- and nighttime capability, make its wind data set unprecedented in that it is amenable to global nonmigrating tidal analysis over a range of MLT altitudes.

2.2. Data analysis

In the following, all semidiurnal tidal components (propagation direction/wave number pairs) are identified by using a letter/number combination indicating both propagation direction (w: westward; s: standing; e: eastward) and zonal wave number $s \geqslant 0$. For instance, w1 is the westward propagating nonmigrating semidiurnal component of zonal wave number 1, s0 is the zonally symmetric (standing) oscillation, and e2 is the eastward propagating component of zonal wave number 2. With the same nomenclature, the migrating semidiurnal tide is w2.

The nonmigrating semidiurnal tides are derived exactly as described by Oberheide et al. (2006) for their diurnal counterparts. It is basically a two-dimensional Fourier transform of a 60-day composite data set that is performed in a running mean sense. Amplitudes and phases are assigned to the day in the middle of each 60-day period. Hence, nonmigrating tidal amplitudes and phases presented here must be interpreted in a climatological sense. Short-term tidal variability cannot be resolved. The present analysis covers the time period June 2002–June 2005. Derived amplitudes and phases are averaged into monthly bins to calculate the tidal climatologies. The details of the analysis are not repeated here, but two important specifics need to be outlined: (1) potential zero wind line inconsistencies in the TIDI warm and cold side data prevent an analysis of the migrating (w2) tide because the latter is observed as a zonally symmetric feature in the satellite data (Oberheide et al., 2003) that has been removed; (2) the inherent smoothing in the set-up of the composite data requires a scaling of the tidal amplitudes (phases are not affected).

The uncertainty in the scaling factors introduces a considerable systematic amplitude error (accuracy). Amplitude and phase precisions, on the other hand, are governed by the measurement noise and the asynoptic satellite sampling. The scaling factors and errors are calculated in the same way as described in detail by Oberheide et al. (2006) for the diurnal tides using both model simulations and the measured data. Amplitude accuracy for the semidiurnal tides is 15–20%, amplitude precision is about 0.8 m/s, and phase precision is 2 h (Table 1). The given values are almost independent of latitude and altitude and apply to the tidal climatologies. Hence, they do not reflect tidal variability from one year to another. The use of 60-day composite data significantly reduces the noise level of the tidal amplitudes and phases, in spite of the large TIDI noise error of an individual wind measurement. For the present error estimate, we used individual wind profile errors of 30 m/s during the day and 60 m/s during the night. The expected net effect of the 30% error reduction induced by the algorithm and instrumental mode adjustments described by Killeen et al. (2006) and outlined in Section 2.1 is small and unlikely to exceed 0.1 m/s.

Fig. 1 shows an example for the scaled meridional wind amplitudes at 95 km altitude for 15 February 2004 as a function of latitude and zonal wave number. The amplitude of a single component (w3) exceeds 12 m/s. Note the difference to Fig. 1b in Oberheide et al. (2006) where the unscaled amplitudes were shown. Semidiurnal tidal analysis is limited to the nonmigrating components w4, w3, w1, s0, e1, and e2. Higher wave numbers require very large scaling factors with increasing uncertainties such that they are excluded.

3. Monthly climatologies

Figs. 2–4 show three examples for the derived climatologies: the w4 zonal wind component (Fig. 2), the w3 meridional wind component (Fig. 3), and the w1 meridional wind component (Fig. 4). Amplitudes are given in m/s and phases are given in universal time (h) of maximum amplitude at 0° longitude. For space reasons, it is impossible to include figures for all 12 components. Instead, amplitude time-series for all components at selected altitudes are shown in Section 5. Numerical amplitude and phase values are available on the web (http://www.atmos.physik.uni-wuppertal.de/cawses/nmt_mlt/).

The w4 zonal wind component (Fig. 2) maximizes in boreal winter around 30–40° North and South. The observed maximum amplitude at 105 km is on the order of 10 m/s but with the peak altitude in most cases well above the upper boundary of the analyzed height interval. Vertical wavelengths during boreal winter are on the order of 40 km and

Table 1
Semidiurnal amplitude and phase errors for the meridional (v) and zonal (u) wind

Component	Scaling factor		Amplitude accuracy		Amplitude precision		Phase precision	
	v	u	v (%)	u (%)	v (m/s)	u (m/s)	v (h)	u (h)
w4	1.50	1.54	17	14	0.8	0.7	1.8	1.6
w3	1.27	1.25	19	17	0.8	0.7	2.0	2.0
w1	1.29	1.33	17	23	0.9	0.7	2.0	1.9
s0	1.51	1.54	13	18	0.8	0.6	2.0	2.0
e1	2.05	2.10	20	13	0.7	0.5	2.2	2.0
e2	3.22	3.10	13	17	0.8	0.6	2.3	1.7

For scaling factors see text.

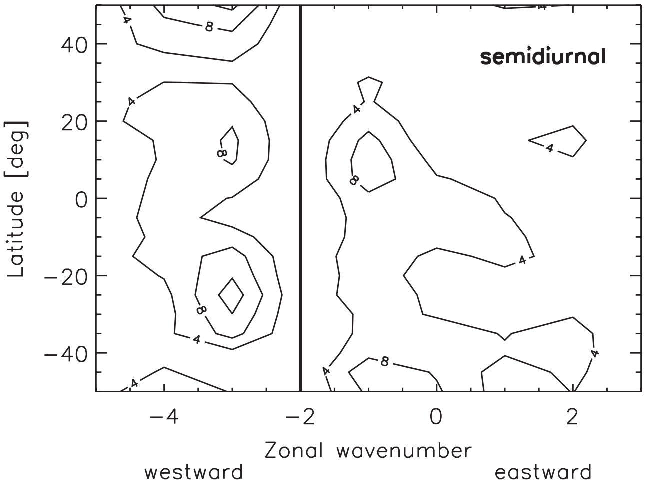

Fig. 1. Amplitudes from TIDI composite data for the period 15 January 2004–18 March 2004 (later assigned to 15 February 2004) at 95 km for the meridional wind. The position of the migrating component (that has not been analyzed) is indicated by the thick vertical line.

the phases decrease with increasing height. This is consistent with upward wave propagation and thus tidal forcing lower in the atmosphere. Between October and March, the phases are symmetric about the equator, that is, the tidal wind directions in the Northern and Southern Hemispheres are the same. During the remainder of the year, the phases are more variable but because the corresponding amplitudes are rather small (except for latitudes poleward of 40°S), it is difficult to decide whether this variability is real or not.

The w3 meridional wind component (Fig. 3) has maximum amplitudes of 8–10 m/s at 105 km. Its peak altitude is usually above the upper boundary of the analyzed height interval. Largest amplitudes are observed one month before spring and fall equinoxes in March and September with maxima at 40° South and North. Boreal winter amplitudes are still large with smaller values in boreal summer (2–5 m/s). An equatorial maximum persists during the whole year. This three peak structure as function of latitude is reflected in the phases that show rapid transitions around 20° North and South where the corresponding amplitudes minimize. The equatorial wind direction is opposite to that at 40° such that tidal up- or downwelling around 20° latitude is likely, due to mass conservation. Again, the phase decrease with height indicates a tidal forcing lower in the atmosphere. Estimating the vertical wavelength is difficult but it is usually on the order of 40 km or above.

The w1 meridional wind component (Fig. 4) maximizes between September and April (up to 10 m/s) with usually four peaks that are located at or slightly poleward of 45° and at roughly 20°. In these cases, three phase jumps at the equator and at 30° North and South occur. If only three peaks are present (i.e., November–January above 95 km), the 20° maxima vanish and an equatorial maximum is observed instead. The phase structure changes accordingly. High latitude amplitudes usually peak above 105 km and thus above the upper limit of the analyzed height interval. Amplitudes between May and August are smaller and patchy. Phases decrease with height but the analyzed height interval is too small to derive a reliable vertical wavelength.

The large variability of the nonmigrating semidiurnal tides in Figs. 2–4 and of many of the components not shown (see Section 5 for time-series) makes their further analysis quite difficult. This particularly applies to the months with small amplitudes when the tidal structure is of course more sensitive to external disturbances. Nevertheless, both the amplitudes and phases show in most cases coherent structures within the error bars (Section 2.2). This and the following comparison with independent measurements may give additional confidence in the derived tidal fields.

4. Comparison with UARS

Angelats i Coll and Forbes (2002) provide w1 and w3 meridional wind climatologies from HRDI and WINDII data (in the following referred to as UARS data). Although their analysis was limited to 95 km altitude and did not include the zonal winds, it is nevertheless an important data set to compare with. The UARS data represent monthly averages of the December 1991 through September 1994 period. Hence, the TIDI comparison with UARS does not meet the hard requirements of validation. The measurements are almost 11 years apart in time. This might be acceptable for climatologies that are taken during the same phase of the solar cycle, but there may or may not have been long-term changes in the MLT region and in the lower atmospheric sources. In addition, validation would also require comparisons with data obtained using different measuring techniques.

However, a TIDI/UARS comparison is certainly helpful to verify the general consistency of both data

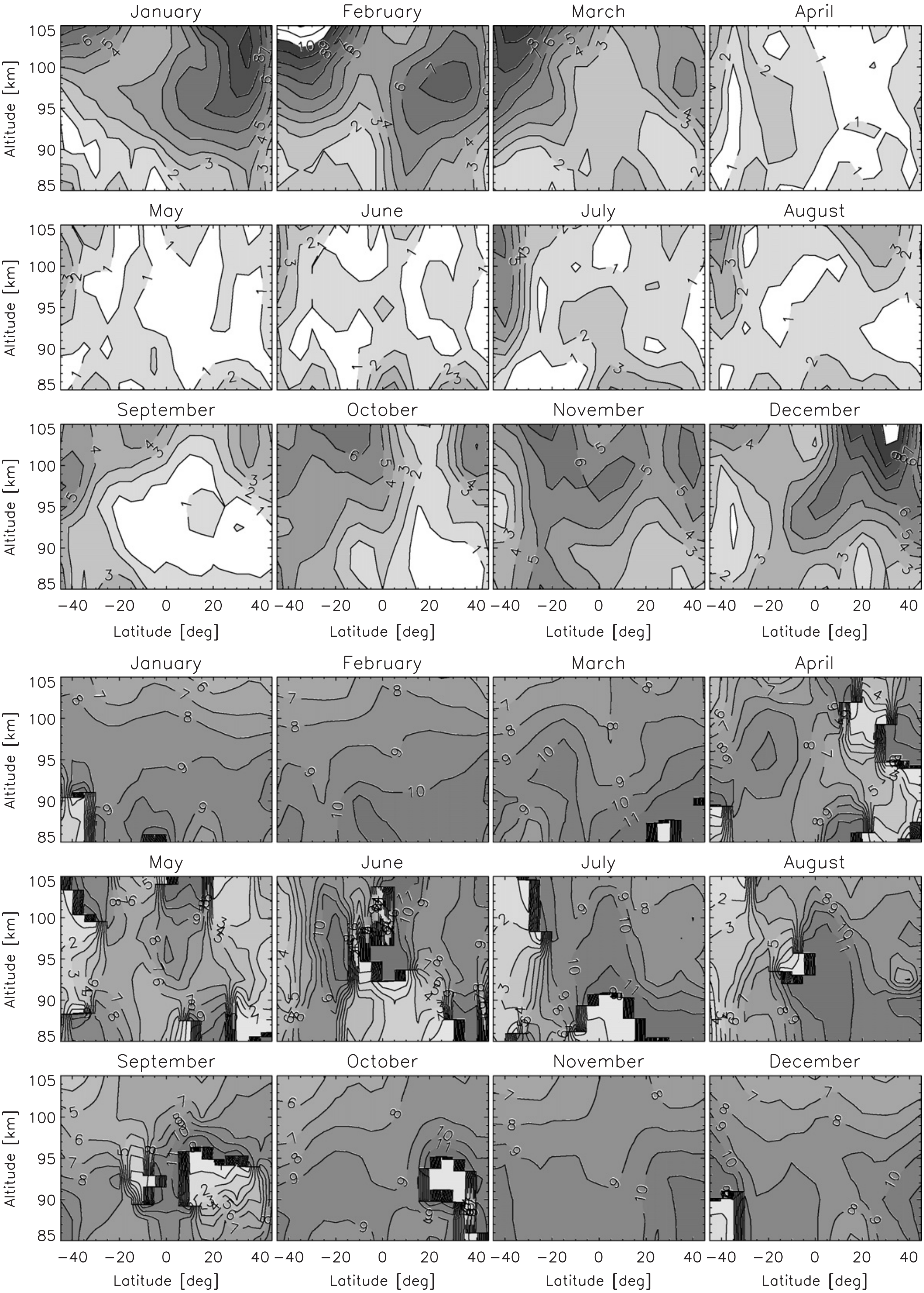

Fig. 2. Monthly mean semidiurnal amplitudes (m/s, top) and phases (Universal time of maximum at 0° longitude in hours, bottom) for the w4 zonal wind component. Multiple phase contours adjacent to each other indicate the transition from 0 to 12 h. Contour intervals are 1 m/s and 1 h, respectively.

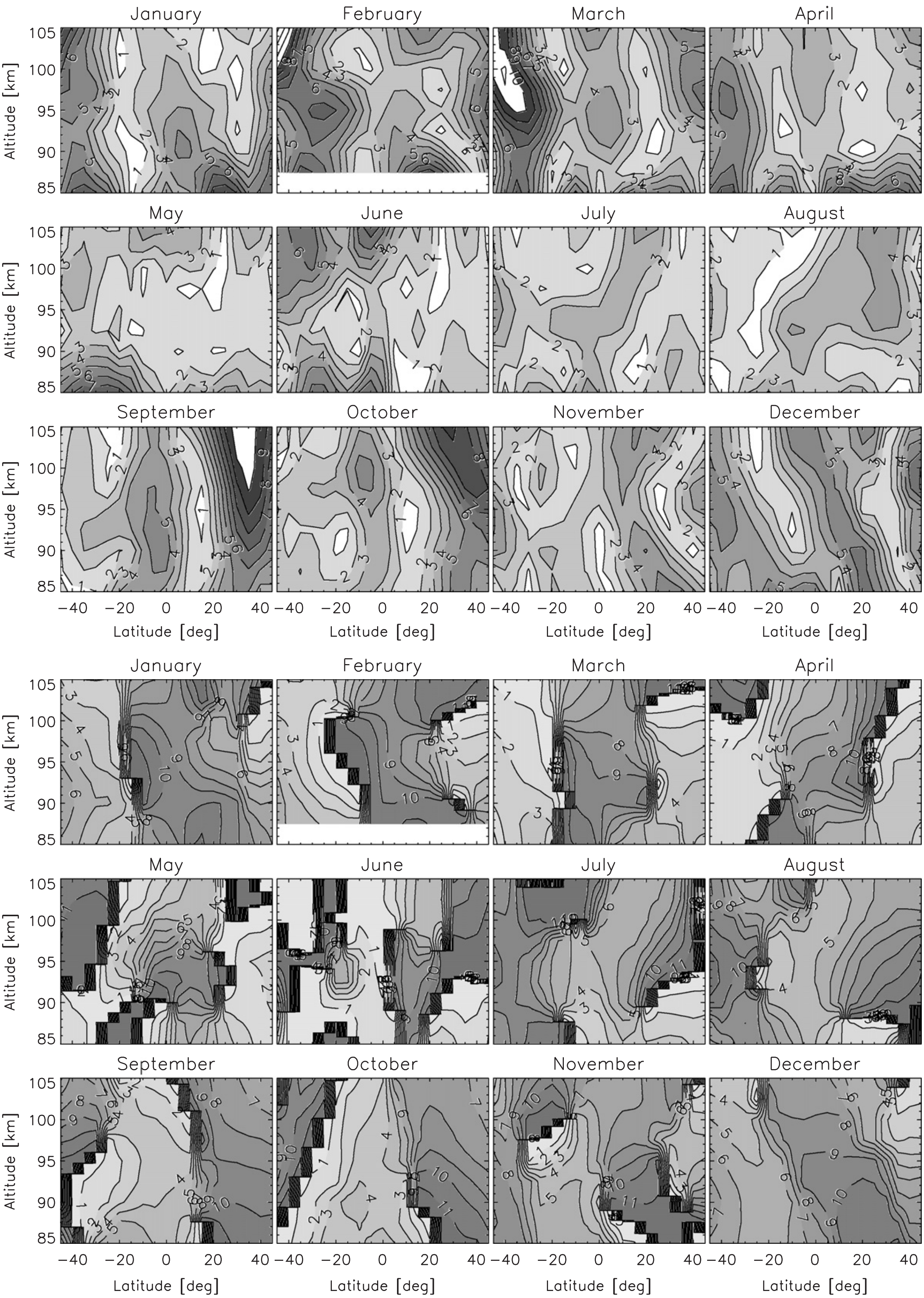

Fig. 3. As Fig. 2, but for the w3 meridional wind component.

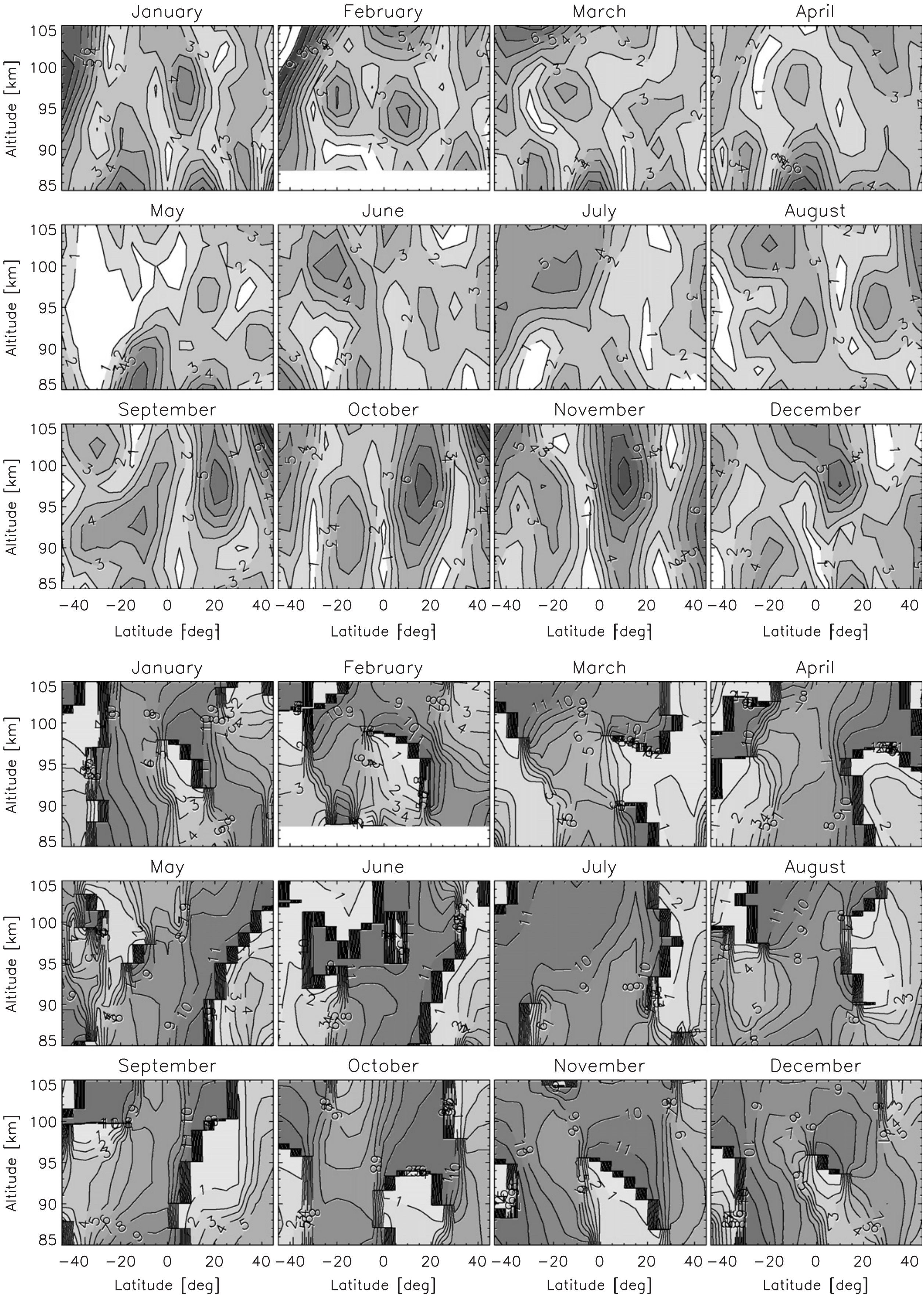

Fig. 4. As Fig. 3, but for the w1 meridional wind component.

sets. A similar comparison for the diurnal tides (Oberheide et al., 2006) yielded an excellent agreement in the spatio-temporal structure at 95 km although the UARS amplitudes were roughly 50% smaller than those from TIDI. Fig. 5 shows the amplitude comparison for the w3 component in January, April, July, and October. TIDI and UARS amplitudes range from almost 0 to 8 m/s with a similar latitudinal distribution in most cases. The UARS minimum at 0° and the maximum at 30°N in January are not observed by TIDI but this is not of much concern because the UARS amplitudes in February (not shown) are very similar to the January and February amplitudes from TIDI. It may thus be related to the 11-year time lag between both data sets. TIDI and UARS amplitudes in April have three maxima that are located within about 10° latitude. The July comparison shows large amplitudes poleward of 40°S in both data sets, a second maximum at low Northern latitudes and another one poleward of 20°N. Latitudes of minimum amplitudes differ by 10° only. In October, the UARS maximum in the Northern Hemisphere is 20° poleward of the TIDI observation but the UARS and TIDI amplitudes behave nevertheless similar: amplitudes increase poleward and equatorward of 40°S, and toward higher Northern latitudes. Because the UARS error bars are unknown, it is difficult to assess whether the amplitude difference in the Northern Hemisphere is significant or not.

The TIDI/UARS comparison for w1 (Fig. 6) is even better. Both data sets show almost the same latitudinal distribution in January, April, and October. The comparison in July is less favorable but becomes better in August (not shown). A more quantitative assessment than discussing pattern similarities is not meaningful here, owing to the 11-year time lag between the measurements. Considering that, the amplitude agreement between TIDI and UARS is rather remarkable. Angelats i Coll and Forbes (2002) established that the non-linear interaction between the migrating tide and the Quasi-Stationary Planetary Wave 1 (QSPW-1) significantly contributes to the generation of the w3 and w1 components observed in the 95 km UARS data. Hence, the same process will likely be of importance in forcing the tides observed in the TIDI data. The relative importance of other mechanisms, that is, the latent heat source, and the height dependence of their imprints upon the tidal fields in the MLT needs further consideration and requires the comparison with models that account for these sources.

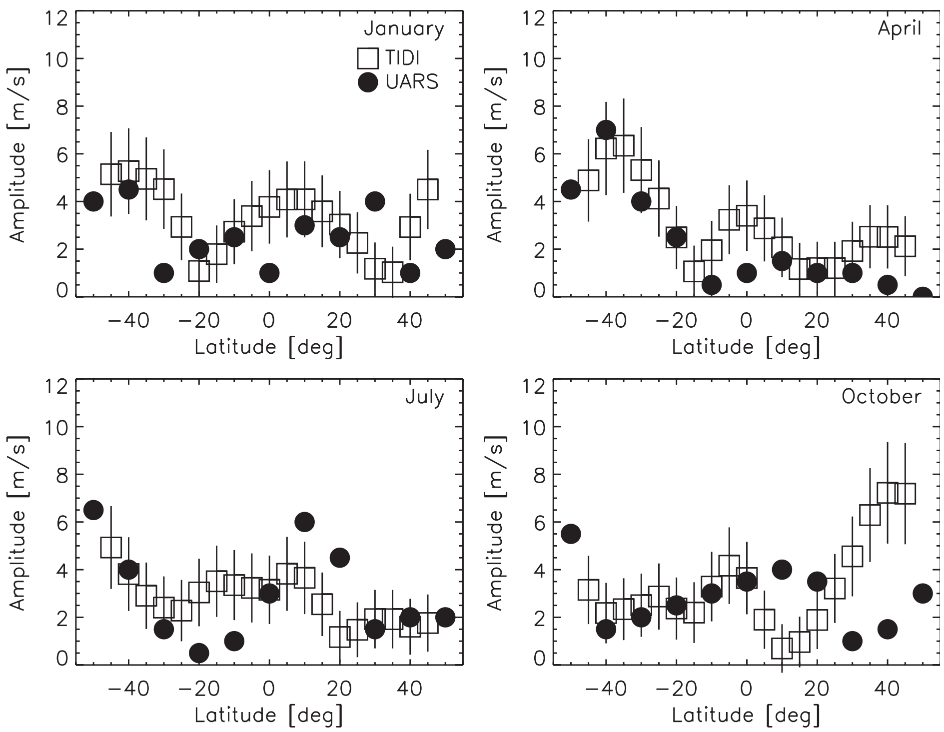

Fig. 5. The w3 meridional wind amplitudes from TIDI and UARS (Angelats i Coll and Forbes, 2002) at 95 km for equinox and solstice conditions. TIDI error bars are from Table 1. UARS error bars are unknown.

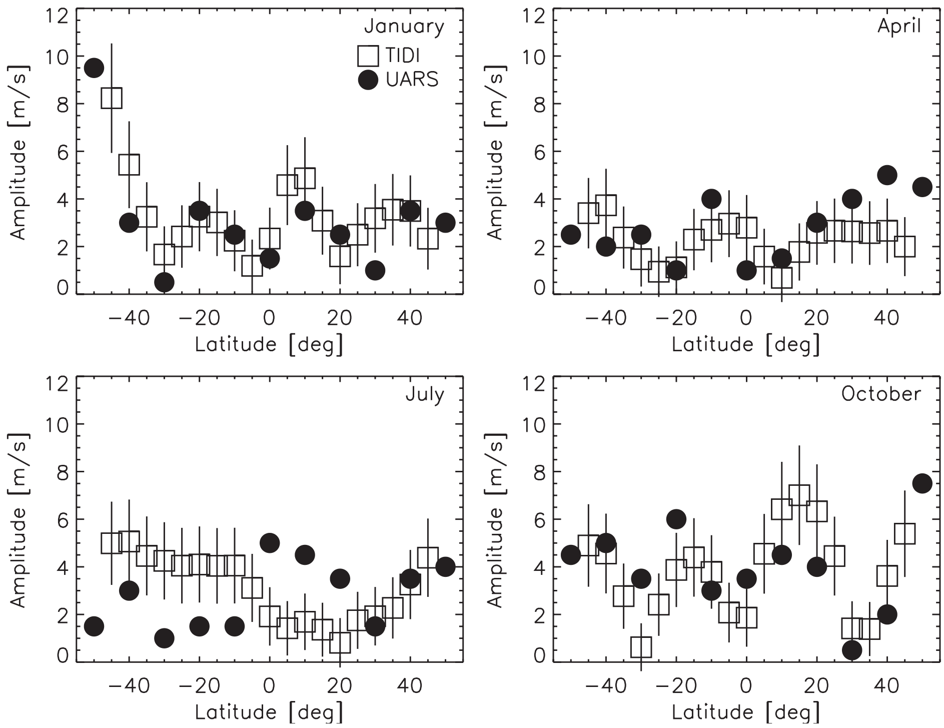

Fig. 6. As Fig. 5, but for the w1 meridional component.

Table 2
Tidal forcing as derived from the observation/model comparison

Component	Forcing
w4	Inconclusive; poor model agreement
w3	Latent heat and wave–wave interaction about equally important
w1	-do-
s0	-do-
e1	Latent heat more important
e2	Latent heat alone

5. Model comparison and tidal forcing

A comparison of the TIDI climatologies to the tidal predictions of the GSWM and the TIME-GCM allows an interpretation of the observational results in terms of forcing mechanisms (Table 2), and, in addition, provides a general assessment of their tidal prediction capabilities. Both the GSWM and TIME-GCM data used in the following come from the same model runs that were used for the diurnal analyses of Oberheide et al. (2006). GSWM is a climatological, linear tidal model that provides monthly amplitudes and phases for 13 diurnal and 13 semidiurnal tidal components (w6 to e6). It does not produce interannual variations and it does not include nonlinear processes such as wave–wave interaction. The only tidal source is latent heat release in the tropical troposphere due to deep convection (Hagan and Forbes, 2003).

The latent heat source is not included in TIME-GCM. Nonmigrating semidiurnal tides in TIME-GCM can only come from wave–wave interactions and/or radiative forcing. Hence, both models account for different tidal sources and may therefore provide insight into the relative importance of the different forcing mechanisms. As for the nonmigrating diurnal tides (Hagan and Roble, 2001), it is reasonable to assume that the nonmigrating semidiurnal TIME-GCM response is primarily driven by the interaction between QSPW-1 and the migrating tide. Zonal asymmetries in ozone and thus in UV absorption may also contribute but they likely do not play a leading role in the model. TIME-GCM was run for the years 2002 and 2003 with realistic solar and geomagnetic forcing. The lower model boundary was specified by GSWM migrating tides (radiative forcing only) and 10 hPa temperature and geopotential data from NCEP. Tidal amplitudes and phases are derived from the daily model output (1 h time resolution) and finally averaged into monthly bins.

Measured and modeled wind amplitudes are now compared as a function of month and latitude (Figs. 7–12). The shown altitudes differ from one

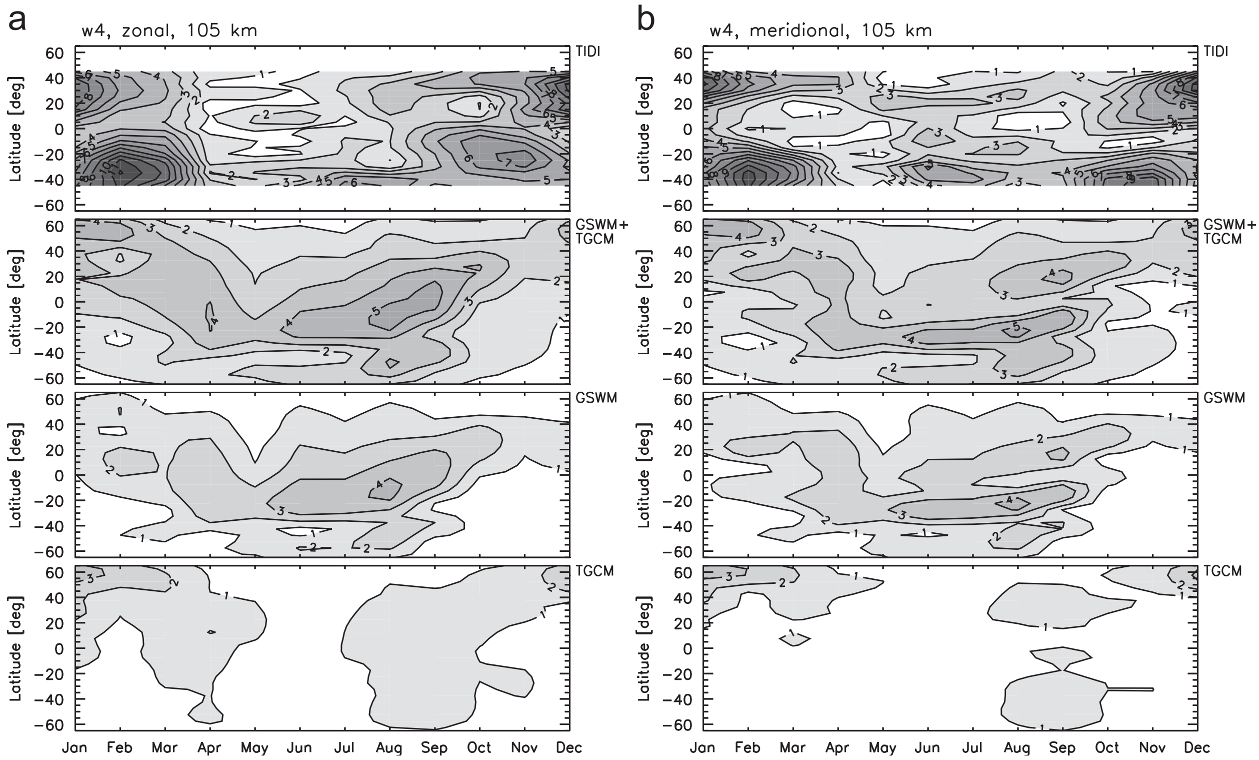

Fig. 7. Latitude-time series of w4 amplitudes at 105 km. From top to bottom: TIDI, sum of GSWM and TIME-GCM, GSWM, TIME-GCM. (a) Zonal wind and (b) meridional wind. Contour interval is 1 m/s.

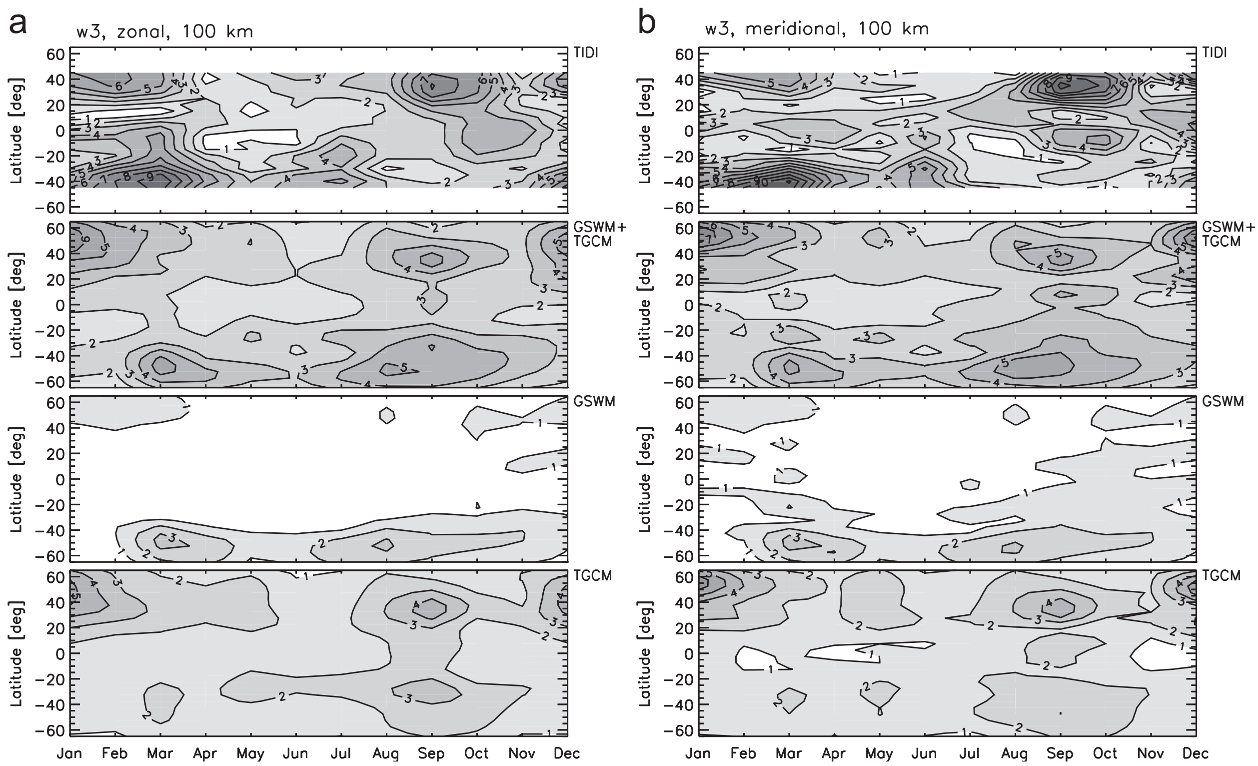

Fig. 8. As Fig. 7, but for w3 at 100 km.

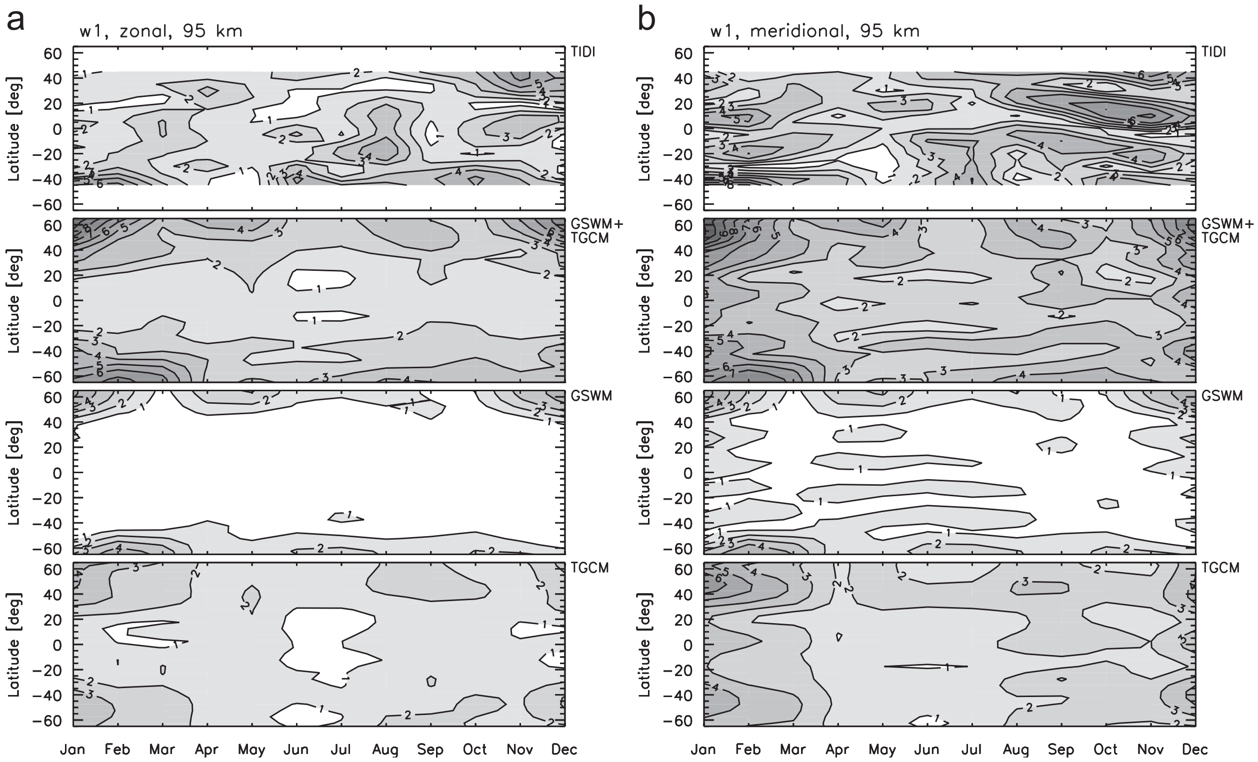

Fig. 9. As Fig. 7, but for w1 at 95 km.

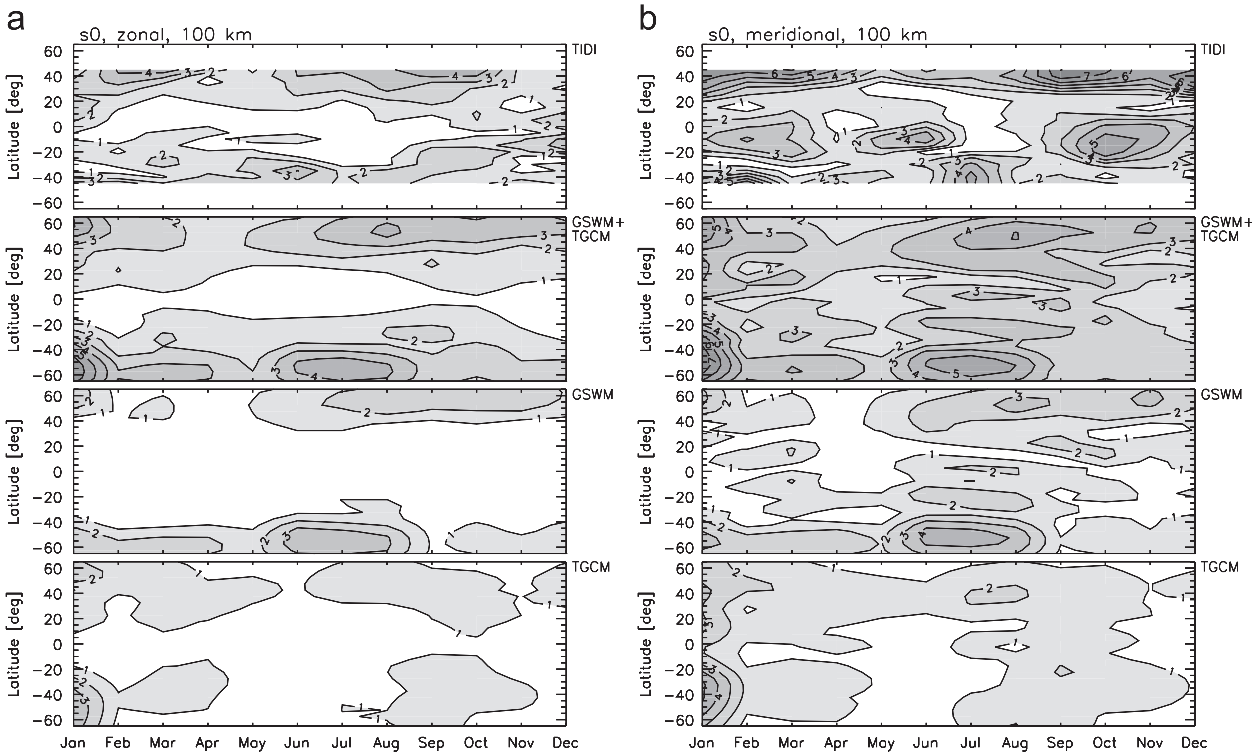

Fig. 10. As Fig. 7, but for s0 at 100 km.

component to another. They reflect the altitudes where the basic features of the respective components are most pronounced. The sum of the GSWM and TIME-GCM amplitudes (without accounting for the relative phasing of both models) is also provided and may be considered as a proxy for the

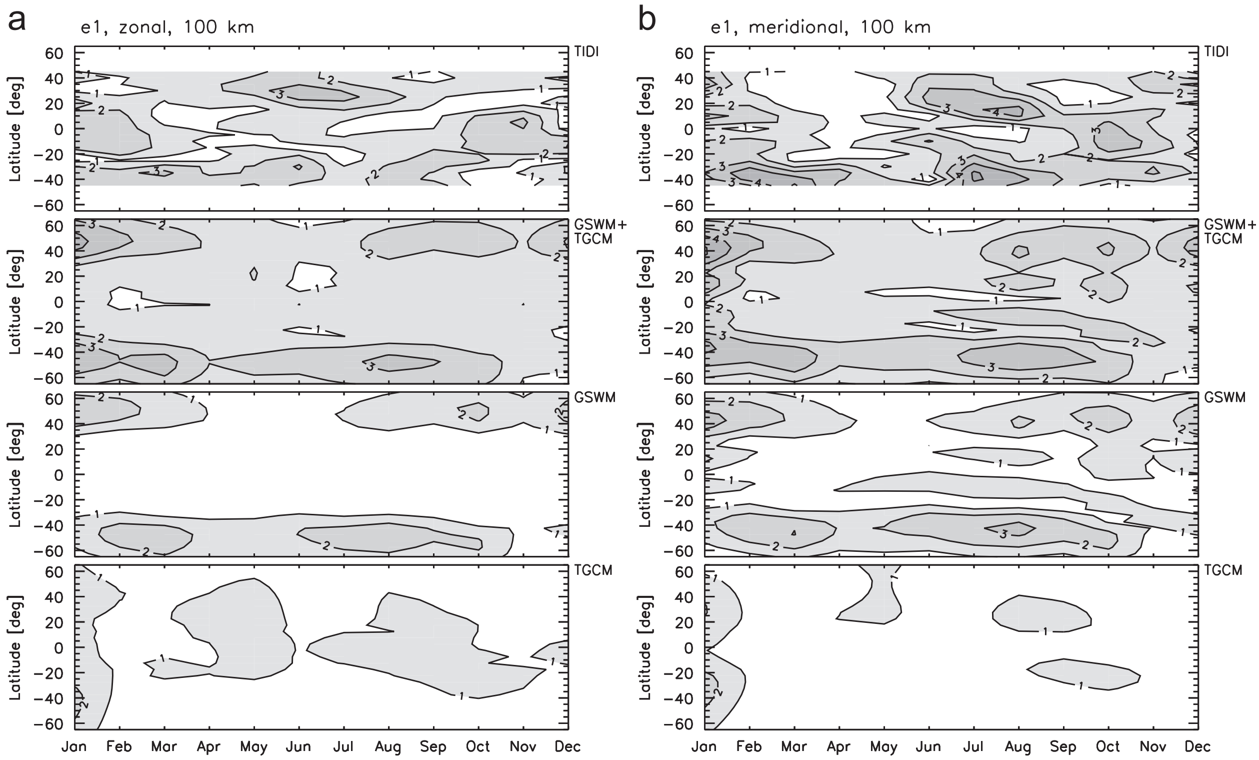

Fig. 11. As Fig. 7, but for e1 at 100 km.

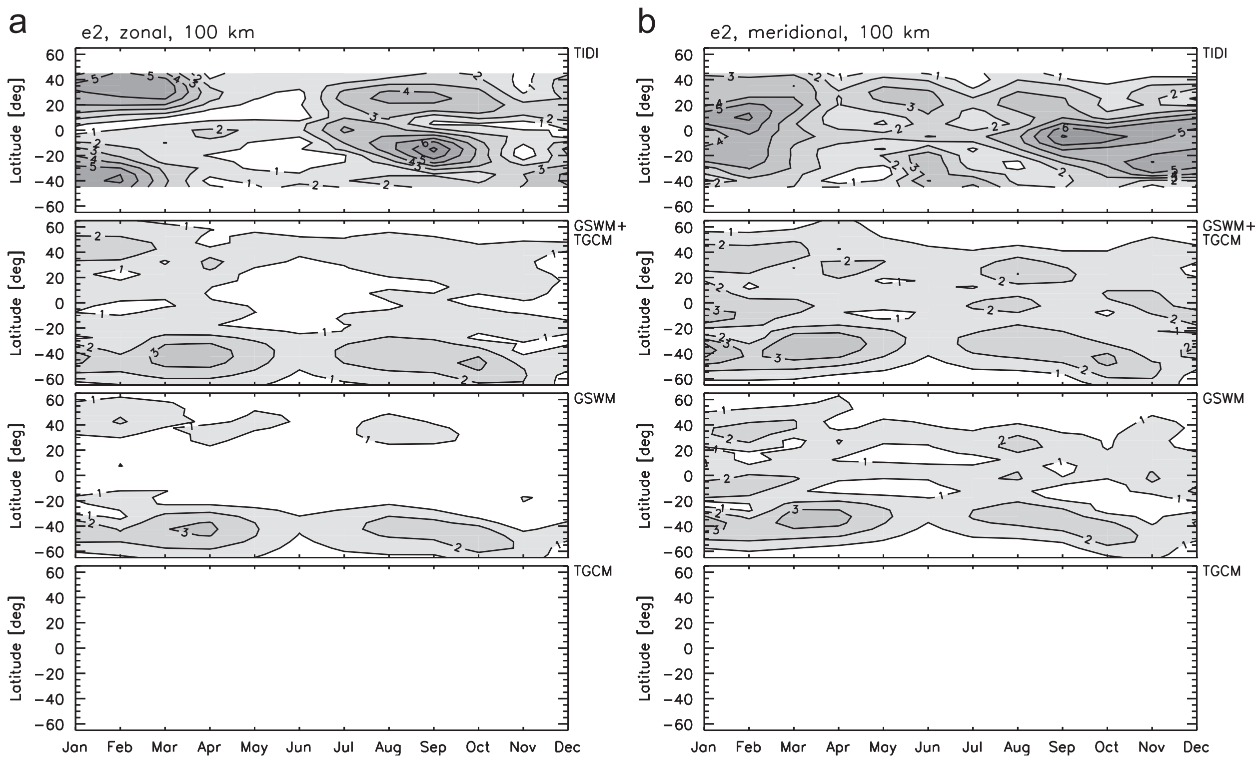

Fig. 12. As Fig. 7, but for e2 at 100 km.

aggregate effects of latent heat release and wave–wave interaction forced tides, as predicted by the models. It is quite obvious that the general result is rather inconclusive. The agreement ranges from good (w3, s0) to moderate (w1, e1, e2) to poor (w4) thus emphasizing the present achievements and shortcomings in understanding the nonmigrating semidiurnal tides. The comparisons with TIDI nevertheless give at least an idea of what sources are important in forcing the various tidal components.

w4 (Fig. 7). Both the GSWM and the TIME-GCM fail to reproduce the observed double peak structure at 30–40° North and South. TIME-GCM maximizes at roughly the same time of the year but with amplitudes that are way too small. GSWM, on the other hand, predicts a low latitude maximum around boreal summer that is only covertly present in the TIDI data during May and June. The model result that latent heat forcing is comparatively more important than wave–wave interaction is thus not confirmed by the observation.

w3 (Fig. 8). The w3 comparison is much better. GSWM and TIME-GCM together reproduce the observed seasonal amplitude variation with maxima around equinoxes and boreal winter and capture the equatorial maximum in the meridional wind quite well. However, neither model predicts the boreal summer peaks in TIDI and they underestimate the observed amplitudes by about a factor of two. Apart from these differences and the general model tendency to peak more poleward, the observation is consistent with the model result that both latent heat release and wave-wave interaction are about equally important in forcing the w3 component over the course of the year. TIME-GCM response is likely caused by migrating tide (w2)–QSPW-1 interaction that can produce w1 and w3 as secondary waves.

w1 (Fig. 9). In the zonal wind, both models reproduce the seasonal amplitude variation at higher latitudes reasonably well with roughly the same contributions. The major difference is the absence of the observed low-latitude maxima. Such a maximum is weakly present in TIME-GCM at 105 km altitude (September, not shown) but in any case much too small compared to TIDI. The models do better in reproducing the latitudinal structure in the meridional wind: the observed four-peak structure is quite evident during most parts of the year. As for w3, GSWM and TIME-GCM show a tendency to peak more poleward compared to TIDI. Observed and modeled amplitudes have about the same magnitude.

s0 (Fig. 10). Zonal wind magnitude and seasonal variation of the combined GSWM and TIME-GCM amplitudes agree quite well with the TIDI result. Again, both models maximize at latitudes more poleward than in the observation. In the meridional wind, the models lack the observed fall equinox maxima but basically capture the occurrence of low latitude maxima although the latter are more pronounced in TIDI. GSWM accounts for about two third of the total model amplitudes. Hence, latent heat release in the tropical troposphere is the comparatively more important tidal source. TIME-GCM response may either come from w2–QSPW-2 interaction and/or w1–QSPW-1 interaction. A recent paper by Liu et al. (2007) suggests that interactions between nonmigrating tides and QSPWs may lead to substantial secondary wave generation in TIME-GCM, at least for the diurnal tides.

e1 (Fig. 11). The modeled zonal wind amplitudes from GSWM and TIME-GCM are quite different: the former predicts two peaks at 50° latitude and the latter one a smaller maximum around the equator. Similar patterns can be found in the TIDI data, although the temporal evolution of the observed small equatorial amplitudes is different. However, the combined model amplitudes agree well with TIDI in the Southern Hemisphere. In contrast to that, the observed temporal evolution in the Northern Hemisphere (boreal summer maximum) is different to the modeled one (boreal summer minimum). For the meridional wind, the combined models predict about the right latitudinal distribution, but with a similar shortcoming as in the zonal wind: the observed boreal summer maximum is not present in the models. The comparison indicates that the e1 response at higher latitudes is governed by latent heat release and the response at lower latitudes by wave–wave interaction. As for s0, the latter would require secondary wave interaction between nonmigrating tides and QSPWs.

e2 (Fig. 12). TIME-GCM response is negligible (smaller than 1 m/s) such that this component is largely driven by latent heat release alone. The predicted (GSWM) maximum in fall occurs simultaneously to the observed one with the winter/spring maximum in TIDI occurring somewhat earlier than in the model. GSWM underestimates the e2 amplitude by roughly a factor of two. The model, although peaking slightly more poleward than the observation, reproduces the boreal winter peak latitudes in the zonal wind quite well. However, the observed zonal wind maxima in fall are located at lower latitudes compared to the model prediction. The boreal summer maximum in the meridional wind has no complement in the model. In addition, TIDI has the largest meridional wind amplitudes at the equator, whereas the model amplitudes at 40° and the equator are about equal.

One possible reason for the model/observation discrepancies and the partly inconclusive results might be that the approach does not account for the effects of latent heat forced nonmigrating tide–QSPW interaction. Tidal forcing and dissipation schemes may also play an important role. With the abovementioned constraints, Table 2 summarizes the forcing as it comes out of the comparisons with GSWM and TIME-GCM.

6. Summary and conclusions

The TIDI wind data allow for the first time a detailed analysis of the morphology of nonmigrating semidiurnal tides over a range of MLT altitudes. Monthly climatologies for six components in the zonal and meridional wind directions have been derived between 85 and 105 km altitude. The present analysis covers the latitude range between 45°S and 45°N and will likely be extended to higher latitudes (60°) in the future, although planetary wave aliasing may become an issue there. At 95 km, the TIDI results agree remarkably well with 1991–1994 results from UARS. During boreal winter, amplitudes of a single component can easily reach 10 m/s such that the aggregate effects of all nonmigrating tides may reach or even exceed the magnitude of the migrating tide although the latter could not be analyzed.

A comparative analysis with the tidal predictions of two models of differing characters, the GSWM and the TIME-GCM, indicates that wave–wave interaction forcing and latent heat release in the tropical troposphere are about equally important in forcing the w3, w1, and s0 components. The eastward propagating components are primarily forced by latent heat release, similar to the findings for the diurnal components (Oberheide et al., 2006). There are, however, several shortcomings in our present model understanding of the semidiurnal nonmigrating tides that lead to model/observation discrepancies that are generally larger than those for the diurnal tides. Reasons for that need to be studied in more detail in the future, but both the interaction between latent heat release forced tides and QSPWs and the model parameterization schemes likely play a role. Results from the ongoing Climate and Weather of the Sun–Earth System (CAWSES) global observing campaign on tides together with the TIDI climatologies and similar analyses of SABER temperatures are expected to give some guidance for future model improvements.

It is nevertheless quite clear that nonmigrating tides provide an effective mechanism to transport the signal of large scale weather systems from the troposphere into the MLT region where they play a decisive role in driving the MLT dynamics. E-region dynamo electric field modulation may then further transport the tidal signal into the F-region. Observational and modeling efforts to understand this vertical coupling over an altitude range of 400 km are still in an early stage but the tidal climatologies from TIDI and SABER will certainly help to get a better hold on the underlying physics in the future.

Acknowledgments

We wish to thank H.-L. Liu for comments on an initial draft of this manuscript. J. Oberheide's work is supported by the DFG priority program CAWSES through Grant OB 299/2-1. The National Center for Atmospheric Research is sponsored by the NSF.

References

Angelats i Coll, M., Forbes, J.M., 2002. Nonlinear interactions in the upper atmosphere: The $s = 1$ and $s = 3$ nonmigrating semidiurnal tides. Journal of Geophysical Research 107 (A8).

Baumgaertner, A.J.G., Jarvis, M.J., McDonald, A.J., Fraser, G.J., 2006. Observations of the wavenumber 1 and 2 components of the semi-diurnal tide over Antarctica. Journal of Atmospheric and Solar-Terrestrial Physics 68 (11), 1195–1214.

Cierpik, K.M., Forbes, J.M., Miyahara, S., Miyoshi, Y., Fahrutdinova, A., Jacobi, C., Manson, A., Meek, C., Mitchell, N.J., Portnyagin, Y., 2003. Longitude variability of the solar semidiurnal tide in the lower thermosphere through assimilation of ground- and space-based wind measurements. Journal of Geophysical Research 108 (A5), 1202.

Forbes, J.M., Wu, D., 2006. Solar tides as revealed by measurements of mesosphere temperature by the MLS experiment on UARS. Journal of the Atmospheric Sciences 63 (7), 1776–1797.

Forbes, J.M., Portnyagin, Yu.I., Makarov, N.A., Palo, S.E., Merzlyakov, E.G., Zhang, X., 1999. Dynamics of the lower thermosphere over South Pole from meteor radar wind measurements. Earth, Planets and Space 51 (7–8), 611–620.

Forbes, J.M., Zhang, X., Ward, W.E., Talaat, E.R., 2003. Nonmigrating diurnal tides in the thermosphere. Journal of Geophysical Research 108 (A1), 1033.

Forbes, J.M., Russell, J., Miyahara, S., Zhang, X., Palo, S., Mlynczak, M., Mertens, C.J., Hagan, M.E., 2006. Troposphere–thermosphere tidal coupling as measured by the

SABER instrument on TIMED during July–September 2002. Journal of Geophysical Research 111 (A10), A10S06.

Grieger, N., Volodin, E.M., Schmitz, G., Hofmann, P., Manson, A.H., Fritts, D.C., Igarashi, K., Singer, W., 2002. General circulation model results on migrating and nonmigrating tides in the mesosphere and lower thermosphere. Part I: comparison with observations. Journal of Atmospheric and Solar-Terrestrial Physics 64 (8–11), 897–911.

Hagan, M.E., Forbes, J.M., 2002. Migrating and nonmigrating diurnal tides in the middle and upper atmosphere excited by tropospheric latent heat release. Journal of Geophysical Research 107 (D24), 4754.

Hagan, M.E., Forbes, J.M., 2003. Migrating and nonmigrating semidiurnal tides in the upper atmosphere excited by tropospheric latent heat release. Journal of Geophysical Research 108 (A2), 1062.

Hagan, M.E., Roble, R.G., 2001. Modeling the diurnal tidal variability with the National Center for Atmospheric Research thermosphere–ionosphere–mesosphere–electrodynamics general circulation model. Journal of Geophysical Research 106, 24,869–24,882.

Hibbins, R.E., Espy, P.J., Jarvis, M.J., 2006. Mean winds and tides in the mesosphere and lower thermosphere above Halley Antarctica. Journal of Atmospheric and Solar-Terrestrial Physics 68 (3–5), 436–444.

Huang, F.T., Reber, C.A., 2004. Nonmigrating semidiurnal and diurnal tides at 95 km based on wind measurements from the High Resolution Doppler Imager on UARS. Journal of Geophysical Research 109 (D10110), doi:10.1029/2003JD004442.

Immel, T.J., Sagawa, E., England, S.L., Henderson, S.B., Hagan, M.E., Mende, S.B., Frey, H.U., Swenson, C.M., Paxton, L.J., 2006. Control of ionospheric morphology by atmospheric tides. Geophysical Research Letters 33 (15), L15108.

Killeen, T.L., Wu, Q., Solomon, S.C., Ortland, D.A., Skinner, W.R., Niciejewski, R.J., Gell, D.A., 2006. TIMED Doppler Interferometer: overview and recent results. Journal of Geophysical Research 111, A10S01.

Lau, E., Avery, S.K., Avery, J.P., Palo, S.E., Makarov, N.A., 2006. Tidal analysis of meridional winds at the South Pole using a VHF interferometric meteor radar. Journal of Geophysical Research 111, D16108.

Lieberman, R.S., Oberheide, J., Hagan, M.E., Remsberg, E.E., Gordley, L.L., 2004. Variability of diurnal tides and planetary waves during November 1978–May 1979. Journal of Atmospheric and Solar-Terrestrial Physics 66, 517–528.

Liu, H.-L., Li, T., She, C.-Y., Oberheide, J., Wu, Q., Hagan, M.E., Xu, J., Roble, R.G., Mlynczak, M.G., Russell III, J.M., 2007. Comparative study of short term tidal variability. Journal of Geophysical Research, in press.

Manson, A.H., Meek, C., Hagan, M., Zhang, X., Luo, Y., 2004. Global distributions of diurnal and semidiurnal tides: observations from HRDI-UARS of the MLT region and comparison with GSWM-02 (migrating, nonmigrating components). Annales Geophysicae 22 (5), 1529–1548.

Mayr, H.G., Mengel, J.G., Talaat, E.R., Porter, H.S., Chan, K.L., 2005. Mesospheric non-migrating tides generated with planetary waves: I. Characteristics. Journal of Atmospheric and Solar-Terrestrial Physics 67 (11), 959–980.

Murphy, D.J., Tsutsumi, M., Riggin, D.M., Jones, G.O.L., Vincent, R.A., Hagan, M.E., Avery, S.K., 2003. Observations of a nonmigrating component of the semidiurnal tide over Antarctica. Journal of Geophysical Research 108 (D8), 4241.

Oberheide, J., Hagan, M.E., Roble, R.G., Offermann, D., 2002. The sources of nonmigrating tides in the tropical middle atmosphere. Journal of Geophysical Research 107 (D21), 4567.

Oberheide, J., Hagan, M.E., Roble, R.G., 2003. Tidal signatures and aliasing in temperature data from slowly precessing satellites. Journal of Geophysical Research 108 (A2), 1055.

Oberheide, J., Wu, Q., Killeen, T.L., Hagan, M.E., Roble, R.G., 2006. Diurnal nonmigrating tides from TIMED Doppler Interferometer wind data: monthly climatologies and seasonal variations. Journal of Geophysical Research 111, A10S03.

Pancheva, D., et al., 2002. Global-scale tidal structure in the mesosphere and lower thermosphere during the PSMOS campaign of June–August 1999 and comparisons with the global-scale wave model. Journal of Atmospheric and Solar-Terrestrial Physics 64 (8–11), 1011–1035.

Roble, R.G., Ridley, E.C., 1994. A thermosphere–ionosphere–mesosphere–electrodynamics general circulation model (TIME-GCM): equinox solar cycle minimum simulations (30–500 km). Geophysical Research Letters 21, 417–420.

Ward, W.E., 1999. A simple model of diurnal variations in the mesospheric oxygen nightglow. Geophysical Research Letters 26, 3565–3568.

Ward, W.E., Fomichev, V.I., Beagley, S., 2005. Nonmigrating tides in equinox temperature fields from the Extended Canadian Middle Atmosphere Model (CMAM). Geophysical Research Letters 32, L03803.

Wu, Q., Killeen, T.L., Nozawa, S., McEwen, D., Guo, W., Solomon, S.C., 2003. Observations of mesospheric neutral wind 12-hour wave in the Northern Polar Cap. Journal of Atmospheric and Solar-Terrestrial Physics 65 (8), 971–978.

Yamashita, K., Miyahara, S., Miyoshi, Y., Kawano, K., Ninomiya, J., 2002. Seasonal variation of non-migrating semidiurnal tide in the polar MLT region in a general circulation model. Journal of Atmospheric and Solar-Terrestrial Physics 64 (8–11), 1083–1094.

Zhang, X.L., Forbes, J.M., Hagan, M.E., Russell, J.M., Palo, S.E., Mertens, C.J., Mlynczak, M.G., 2006. Monthly tidal temperatures 20–120 km from TIMED/SABER. Journal of Geophysical Research 111, A10S08.